



On the factors behind large Labrador Sea tides during the last glacial cycle and the potential implications for Heinrich events

Brian K. Arbic,¹ Jerry X. Mitrovica,² Douglas R. MacAyeal,³ and Glenn A. Milne^{4,5}

Received 17 November 2007; revised 1 April 2008; accepted 1 May 2008; published 1 August 2008.

[1] Labrador Sea (LS) tidal elevations over the last glacial cycle are investigated in a near-global numerical model that accurately captures the present-day tides. From ~ 65 ka to ~ 7 ka, the modeled elevations at the debouchement point of the Hudson Strait ice stream in the LS are exceptionally large, comparable to the largest elevations seen anywhere in the present-day ocean. New numerical simulations performed for this article demonstrate that both local changes in basin geometry (e.g., ice cover over Hudson Bay) and changes outside of the LS led to enhanced LS paleotides. New simulations run at higher horizontal resolution and a considered examination of uncertainties, including uncertainties in the adopted sea level models, strengthen confidence in the robustness of the large LS paleotides. The tide model is run with both spatially uniform sea level drops (taken from curves of eustatic and Red Sea sea levels versus time) and spatially variable sea level maps (taken from two different gravitationally self-consistent viscoelastic solid earth/sea level models, which both account for ice sheet geometry). The tides are larger when the spatially variable sea level models are used. Observations in present-day Antarctica indicate that the mechanical action of tides significantly impacts the dynamics of both continental ice streams and their associated floating ice shelves. It is postulated here that large LS paleotides played a key role in the formation of Heinrich event icebergs, that is, massive discharges of ice from the LS into the glacial North Atlantic ocean. The paleotide calculations described here provide a potential explanation for why the LS region, more than any other, dominated the production of Heinrich event icebergs. Most previous hypotheses of a tidal role in climate variability and ice sheet dynamics focus on tidal mixing. In contrast, here the role of tidal mechanical forcing of ice sheets is emphasized.

Citation: Arbic, B. K., J. X. Mitrovica, D. R. MacAyeal, and G. A. Milne (2008), On the factors behind large Labrador Sea tides during the last glacial cycle and the potential implications for Heinrich events, *Paleoceanography*, 23, PA3211, doi:10.1029/2007PA001573.

1. Introduction

1.1. Overview

[2] This article investigates paleotides during the last glacial cycle using a near-global forward ocean tide model that replicates present-day tidal elevations to a high level of accuracy, coupled with a state-of-the-art model [Milne *et al.*, 1999] (hereafter referred to as MMD) of paleo sea levels. The sea level model puts out global maps of the ocean/land ice boundary and of spatially varying sea levels relative to those of today. Our study is focused on tidal elevations rather than on tidal currents. We pay particular attention to the paleotides of the Labrador Sea (LS) and the factors

behind the changes over time in the tides of that region. Our focus on the LS is motivated by two facts: (1) the modeled paleotides are much larger in the LS than in most other locations and (2) the LS is the main location of Heinrich event iceberg discharges [Hemming, 2004]. As discussed in section 1.4, there is mounting evidence from observations in present-day Antarctica that continental ice sheets and floating ice shelves are impacted by the mechanical action of tides. Motivated by this evidence, we suggest here, as in our recent note [Arbic *et al.*, 2004a] (hereafter referred to as AMMM), that tides played a catalytic role in Heinrich events.

[3] In the current article, we describe more of the details behind our paleotide simulations than space permitted in AMMM. We present a more considered examination of the uncertainties in our paleotide calculations, including a comparison of our results with those of other recent paleotide studies, and an investigation of the sensitivity of the paleotide model to different choices of adopted sea level input. We run new simulations with a different model [Peltier, 2004] of spatially varying sea levels. We discuss in more detail the differences between tide simulations run with spatially varying sea level models and those run with spatially uniform sea level changes. We use two different estimates of the temporal evolution of globally averaged sea

¹Institute for Geophysics, Jackson School of Geosciences, University of Texas at Austin, Austin, Texas, USA.

²Department of Physics, University of Toronto, Toronto, Ontario, Canada.

³Department of Geophysical Sciences, University of Chicago, Chicago, Illinois, USA.

⁴Department of Earth Sciences, University of Durham, Durham, UK.

⁵Now at Department of Earth Sciences, University of Ottawa, Ottawa, Ontario, Canada.

level change. We present a more thorough investigation, involving new numerical simulations, of the factors behind the large LS paleotides. We discuss new simulations, run at higher horizontal resolution, which strengthen our confidence in the robustness of the large LS paleotides predicted by our model. We provide a more substantial discussion of the potential role of ocean tides in Heinrich events, including a comparison of our tidal hypothesis with other hypotheses of a tidal role in millennial climate variability. Finally, we briefly describe the work of *Griffiths and Peltier* [2008, also *Polar ocean tides at the Last Glacial Maximum: Amplification, sensitivity, and climatological implications*, submitted to *Journal of Climate*, 2008], which adds substantially to the discussion of the potential role of tides in ice sheet instabilities during the last ice age.

[4] Another recent study of paleotides [*Egbert et al.*, 2004] focused on tidal dissipation in the last glacial maximum (LGM) and post-LGM ocean. There is great interest in the community [e.g., *Wunsch and Ferrari*, 2004] regarding the role of dissipation and associated mixing in the present day and paleo-ocean circulation. *Egbert et al.* [2004] showed that the tidal dissipation during ice age times, particularly in the abyssal ocean, was significantly larger than it is today. We will not add in this article to the very thorough discussion of paleotidal dissipation in *Egbert et al.* [2004; see also *Uehara et al.*, 2006; *Griffiths and Peltier*, 2008, also submitted manuscript, 2008]. Instead we focus on the large paleotides of the LS, the causes of the large LS paleotides, and the potential implications of the large LS paleotides for ice sheet dynamics.

1.2. Factors Influencing Temporal Changes in the Ocean Tides

[5] There are three main reasons to suspect that tides during glacial times might have been different than they are today. The first reason is that alterations in basin geometry affect tidal resonances. Tides excite resonant normal modes of ocean basins [*Platzman et al.*, 1981] because the travel time for tides to cross basins is comparable to tidal forcing periods. Normal modes near semidiurnal (twice daily) periods have strong signatures in the North Atlantic, which is pertinent for our study. The lower sea levels of glacial times affected tides by lowering tidal phase speeds, which depend on the square root of the water column thickness, and by decreasing the sizes of the basins in which the tides resonate. As will be discussed later, the relative changes in basin sizes and water depths were much greater in shallow areas than in the deep ocean. The second reason to suspect a difference between ice age and present-day tides is that lower sea levels during the ice age led to a reduction in the areal extent of continental shelves, on which about 2/3 of the present-day tidal dissipation takes place [*Egbert and Ray*, 2003]. Since many shallow water regions are reduced in extent or even eliminated with a drop in sea level, the tidal dissipation and therefore the tides themselves would be different under ice age conditions. With our coupled sea level/ocean tide model we can quantitatively account for changes in tidal resonances and in shelf dissipation. It is more difficult for us to accurately account for the third potentially important factor affecting paleotides, namely

alterations in the stratification of abyssal waters, which enters into parameterizations of drag and energy dissipation in the deep ocean. We will examine this third effect with a sensitivity study to be described later.

1.3. Heinrich Events

[6] Over the last 800,000 years, the ice age Earth was subjected to a series of $\sim 100,000$ -year glacial cycles, during which large ice complexes covered northern North America and northern Europe. The ice sheets experienced intermittent instability. The marine sediment record reveals several large pulses of detritus deposited episodically in the North Atlantic during glacial times. These “Heinrich events” [*Heinrich*, 1988; *Broecker et al.*, 1992; *Bond et al.*, 1992; *Grousset et al.*, 1993; *Hemming*, 2004] are thought to represent ice-rafted debris originating mainly from the LS, with a smaller contribution from material of European origin [*Hemming*, 2004]. The meridional overturning circulation in ocean general circulation models is sensitive to the introduction of freshwater inputs [e.g., *Winton and Sarachik*, 1993; *Manabe and Stouffer*, 1995; *Sandal and Nof*, 2008], suggesting a mechanism for Heinrich event icebergs to impact climate on large, perhaps even global, scales. Indeed proxy evidence points to significant and far-reaching impacts of Heinrich events on ice age climate [e.g., *Bard et al.*, 2000; *Broecker and Hemming*, 2001; *Hemming*, 2004]. Internal “binge-purge” dynamics of the Hudson Strait ice stream [*MacAyeal*, 1993], outburst flooding and subsequent ice surges [*Johnson and Lauritzen*, 1995; *Alley et al.*, 2006], changes in ocean heat transport [*Moros et al.*, 2002], a catastrophic breakup induced by meltwater fill of crevasses in the fringing LS ice shelf fed by the Hudson Strait stream [*Hulbe et al.*, 2004], iceberg calving due to remotely generated oceanic swell [*MacAyeal et al.*, 2006], and subsurface oceanic warming and sea level rise [*Flückiger et al.*, 2006] are among the mechanisms advocated for discharge of significant detritus into the North Atlantic ocean from the LS region.

1.4. Labrador Sea Tides and Heinrich Events

[7] As done by AMMM, we point out here another potentially important factor in the dynamics of Heinrich event icebergs (and, more generally, Laurentide ice sheet dynamics throughout the ice age). Our work highlights a specific phenomenon located around the LS, namely, that the LS tides are much larger than those in contact with ice sheets in most other regions, and thus offers a potential explanation for the larger amounts of Hudson Strait detritus in the ice-rafted debris that marks Heinrich events.

[8] Evidence of tidal effects on ice streams and floating ice shelves comes from observations in present-day Antarctica, where signatures of tidally induced ice flexure have been found both at the surface of ice shelves and at the grounding lines of ice streams [*Williams and Robinson*, 1980; *Doake et al.*, 1987; *Smith*, 1991]. Tides are thought to weaken ice shelves by forming crevasses at their hinge lines. Tides modulate the variability of ice flow in floating ice shelves [*Doake et al.*, 2002; *Brunt et al.*, 2006]. Furthermore, the basal seismicity [*Anandkrishnan and Alley*, 1997] and stick-slip flow of ice streams [e.g., *Bindschadler et al.*,

2003] are controlled by tides far upstream of floating ice shelves and their grounding lines. A thorough recent discussion can be found in the work of *Murray et al.* [2007, and references therein], who found through analysis of a long (2-year) time series of ice stream velocity data that there is very little energy at frequencies other than tidal frequencies. They conclude that other possible drivers of ice stream velocity fluctuations do not contribute significantly. Motivated by the mechanical controls of tides on both ice streams and ice shelves, we investigate the evolution of LS tides during the last glacial cycle. We note that tides also impact ice sheets through their role in ocean mixing, which affects the temperatures of seawater in contact with the edges of ice sheet complexes. This latter possibility is not a focus of our article, though we do not dismiss it.

2. Sea Level Model

[9] In order to perform paleotide simulations, we require a model of the temporal evolution, over a glacial cycle, of the spatial distributions of both the ocean/land ice boundaries (referred to as a mask) and of sea level variations. Except where noted, we utilize in this article sea level predictions from the numerical algorithm of MMD and *Mitrovica and Milne* [2003]. The algorithm takes accurate account of changes in shoreline geometry and feedback from perturbations in Earth rotation. The algorithm is gravitationally self-consistent, and gravitational effects will be noted and described in section 4. The viscoelastic Earth model we use is characterized by the elastic structure of the seismic model PREM [*Dziewonski and Anderson*, 1981], an elastic lithospheric plate of thickness 100 km, an upper mantle viscosity of 5×10^{20} Pa s, and a factor of 40 jump in viscosity across the interface (at 670 km depth) between the upper and lower mantle. These choices are consistent with recent inferences of radial viscoelastic Earth structure derived from a suite of independent data sets related to the glacial isostatic adjustment process [*Lambeck et al.*, 1998; *Mitrovica and Forte*, 1997]. The global ice history is constructed to provide a close fit to sea level records in the far field of the ice sheets that span the period subsequent to the last glacial maximum (LGM; ~ 20 ka) [*Bassett et al.*, 2005]. Prior to LGM, we adopt the ice volume time series inferred by *Lambeck et al.* [2002] and assume that ice geometries during the glaciation phase were identical to those within the most recent deglaciation period whenever the ice volumes were equivalent. The algorithm yields a time series of global sea level (relative to present; and geographically varying) and a corresponding ocean/land ice mask. These can be combined with present-day topographic maps (see *Arbic et al.* [2004b] (hereinafter referred to as AGHS) for a description of the construction of these maps; ultimately the data sources from *Smith and Sandwell* [1997]) to reconstruct paleobathymetries at any stage in the glacial cycle. We will also run some simulations with the ICE-5G model of *Peltier* [2004], as well as a suite of simulations with spatially uniform sea level drops taken from the curve of eustatic sea level versus time used in

MMD, and taken from the Red Sea sea level data of *Siddall et al.* [2003].

3. Ocean Tide Model

3.1. Model Description

[10] The most accurate global models of present-day tidal elevations are either empirical models derived from TOPEX/POSEIDON satellite altimetry, or hydrodynamical models that are constrained by either tide gauges or altimetry [e.g., *Egbert et al.*, 1994]. However, models constrained by present-day tides cannot be used to study paleotides. We simulate paleotides here in the one-layer forward model of AGHS. We take the astronomical forcing of the tides to be equal to what it is today. This assumption is valid on the timescales of the last glacial cycle. Except where noted, the simulations shown here were run on a $1/2^\circ$ latitude-longitude grid, over the latitude range 86°S to 82°N . We discuss model sensitivities to the artificial northern boundary (wall) at 82°N later in the article. Most simulations were run with only the largest tidal constituent, namely the principal lunar semidiurnal tide M_2 , which has a period of 12.4 h. Approximately two thirds of the energy, and two thirds of the energy dissipation, of the present-day tides is due to M_2 alone [*Egbert and Ray*, 2003]. A few simulations were performed with multiple tidal constituents, namely, the four largest semidiurnal (M_2 , S_2 , N_2 , K_2) and four largest diurnal (K_1 , O_1 , P_1 , and Q_1) tides. As discussed in AGHS, our $1/2^\circ$ model captures 92% of the sea surface elevation variance in present-day pelagic tide gauge records of these eight constituents, and 91% of the open-ocean elevation variance in present-day satellite-constrained models of these eight constituents.

[11] The main result we will report on in this article is the amplitude of M_2 elevations, shown either in global maps or at a local point of interest in the LS. We will not show maps of tidal phase in this article. At any grid point in the model, the peak-to-peak elevation change due to M_2 is twice the M_2 amplitude. The modeled peak-to-peak tidal range (i.e., the difference between high and low tide) further increases when constituents at other frequencies are included. This is because at certain times of the month (spring tide) the high tides of different large constituents occur at the same time.

3.2. Ocean Tidal Dissipation and Abyssal Stratification

[12] The accuracy of forward tide models has improved recently because of advances in our understanding of tidal dissipation. Analysis of highly accurate satellite-constrained tide models has shown [*Egbert and Ray*, 2003] that 1.0 TW of the total 3.5 TW present-day ocean tidal dissipation takes place in the abyssal ocean, primarily in areas of rough topography, while the remainder of the dissipation takes place in shallow seas. Energy loss in these regions is thought to occur via generation of turbulence and of breaking internal gravity waves by background flows, including tidal flows, over the rough seafloor. Parameterizations of internal wave drag on flow over the rough bottom have recently been implemented in forward tide models, that is, models that are unconstrained by observa-

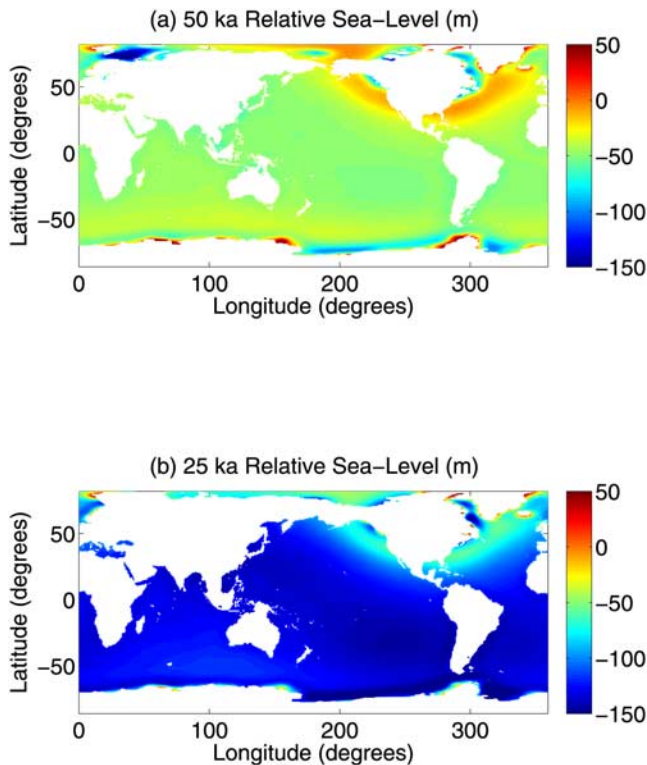


Figure 1. Global maps of ocean/land ice mask and spatially varying relative sea level (m) with respect to present-day values, from the MMD sea level model, at (a) 50 ka and (b) 25 ka.

tions [Jayne and St. Laurent, 2001; Carrère and Lyard, 2003; Egbert et al., 2004; AGHS; Uehara et al., 2006; Lyard et al., 2006; Griffiths and Peltier, 2008, also submitted manuscript, 2008]. Although the schemes used in the various studies differ in detail, they all depend on the stratification $N = \sqrt{-(g/\rho_0)(d\rho/dz)}$ (computed at every model grid point from a climatology, in our case, the Levitus et al. [1998] climatology), where $g = 9.8 \text{ m s}^{-2}$ is gravitational acceleration, ρ_0 is an average seawater density, and $d\rho/dz$ is the vertical (z) derivative of potential density ρ . All the schemes are capable of significantly improving the accuracy of forward-modeled present-day surface tidal elevations.

[13] The wave drag scheme used in AGHS and in some of the other tide models depends in particular on the stratification N in the abyss. Abyssal values of N during the ice ages are poorly known, and we discuss model sensitivities to this important parameter later in the article. Except where noted, simulations shown here are done assuming present-day abyssal N values. We use the topographic drag strength from the AGHS simulations of the present-day tides, in which the drag scheme was tuned with a multiplicative factor that may account for the limited horizontal resolution of small-scale features in available global topographic data sets [Smith and Sandwell, 1997]. At $1/2^\circ$ resolution the optimal multiplicative factor, in terms of minimizing the elevation error with respect to satellite-constrained tide models, is 7. In the AGHS simulations of the present day

as well as in most of the paleo simulations reported on in AMMM and here, we choose to utilize topographic drag only in waters deeper than 1000 m. We will report on some simulations in which topographic drag is utilized in all waters deeper than 100 m. In the latter case, a slightly lower elevation error can be achieved, with a smaller optimal multiplicative factor (5, in $1/2^\circ$ simulations). As we will show, these two different utilizations of topographic drag lead to very similar predictions for the LS paleotides.

[14] For a discussion of earlier attempts (made before the topographic wave drag parameterizations became commonplace) to model global tides over glacial timescales, the reader is referred to Thomas and Sündermann [1999] and references therein. An informative discussion of regional paleotide models run over glacial timescales can be found in the work of Uehara et al. [2006]. For the remainder of this article we will compare our study only to those other recent paleotide studies which also incorporate topographic wave drag [Egbert et al., 2004; Uehara et al., 2006; Griffiths and Peltier, 2008, also submitted manuscript, 2008], all of which focus on tides over glacial timescales.

3.3. Self-Attraction and Loading Term

[15] A major complication of tide models [Hendershott, 1972; Ray, 1998] is that they must accurately account for the self-attraction, or self-gravitation, of the ocean tide, for the deformation of the solid earth due to the loading of tidal mass anomalies, and for the self-gravitation of these solid earth deformations. These effects are by convention gathered into one term, known as the self-attraction and loading (SAL) term. Because the SAL term is a complex and computationally expensive function of the tide itself, it is generally not computed “on the fly” inside a tide model as the model runs. Most tidal studies either employ the “scalar approximation,” in which the SAL term is written as a simple spatially uniform multiple (~ 0.1) of the tidal elevation, or use the scalar approximation as a first guess and then compute the tide and its associated SAL iteratively, with successive computations. Except where noted, throughout this article we employ the second method, and we show and discuss results from the third iteration of the SAL term (two iterations past the so-called scalar approximation). Both Egbert et al. [2004] and AGHS discuss methods, which we adopt here, to improve globally integrated measures of convergence in such iterations.

4. Results of Sea Level and Ocean Paleotide Models

4.1. Results of Sea Level Model

[16] Example maps of relative sea levels (and the ocean/land ice mask) predicted by the viscoelastic sea level model [Milne et al., 1999] described in section 2, at 50 ka and 25 ka, are shown in Figure 1. At high latitudes, gravitational and loading effects, namely, the gravitational pull of the ice sheets on seawater and the compression and rebound of the solid earth under the advance and retreat of the ice sheets, are significant. As a result, the relative sea levels predicted for locations near the high-latitude ice sheets can deviate markedly from the globally averaged (eustatic) values, which are -47.4 and -127.9 m, respectively.

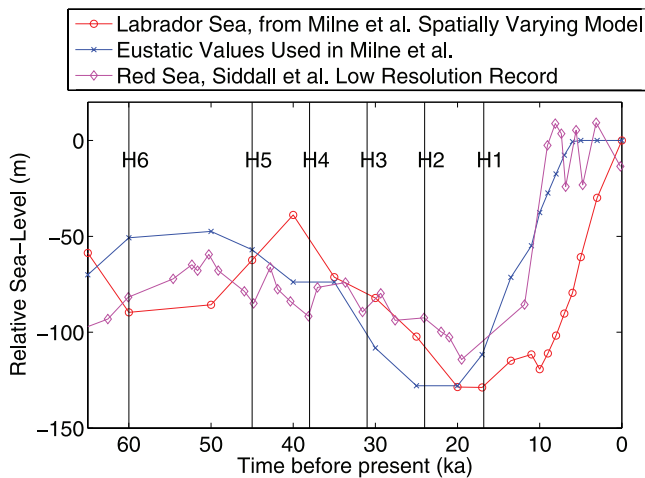


Figure 2. Sea level (m) over the last 65 ka, relative to present day. Values at 61.5°N, 296°E (“Labrador Sea”; taken from spatially varying MMD sea level model), eustatic values used by MMD, and values from the Red Sea [Siddall *et al.*, 2006] are shown. Timings of Heinrich events are shown in black.

[17] The red curve in Figure 2 is the predicted relative sea level over the last 65 ka at 61.5°N, 296°E, the approximate debouchement point of the Hudson Strait ice stream. This site will serve as our representative “Labrador Sea” (LS) location in the article. The timings [Hemming, 2004] of Heinrich events H1–H6 are superimposed on the figure. LS sea level was lower than at present, by ~ 40 –130 m, during these events. The blue curve in Figure 2 is the so-called eustatic sea level curve computed by assuming that the model ice mass variations are accompanied by spatially uniform changes in ocean height. The magenta curve in Figure 2 shows the last 65 ka of the “low-resolution” record of sea level values in the Red Sea [Siddall *et al.*, 2006] (updated version of results in Siddall *et al.* [2003]). Assuming that the Red Sea is representative of much of the globe, we can use the Red Sea record as an alternative to the eustatic curve, in experiments which utilize spatially uniform reductions in sea level. The discrepancy between LS sea level predicted with a gravitationally self-consistent viscoelastic theory and with the eustatic and Red Sea values can reach order 50 m and is characterized by a systematic trend in the post-LGM period.

4.2. Results of Coupled Ocean Tide/Sea Level Model

[18] Figure 3 shows global maps of the modeled M_2 amplitudes at 50 ka and 25 ka, using the relative sea level and ocean/land ice mask output from the viscoelastic MMD sea level model coupled to the forward tide model. For comparison, present-day M_2 amplitudes in the forward model, and in the highly accurate satellite-constrained TPXO6.2 model [Egbert *et al.*, 1994], are shown in Figure 4. The modeled paleo M_2 amplitudes (Figure 3) are much larger in the LS than in most other deep parts of either the paleo- or present-day ocean. The tides in Hudson Strait are among the largest of the present day.

[19] This article focuses on tidal elevations. In both present-day and 25 ka simulations, tidal currents in the LS (not shown) are amongst the largest in the global ocean, but the LS tidal currents in the 25 ka simulation are not greatly enhanced, if at all, over those in the present day.

[20] The red curve in Figure 5 shows the LS M_2 amplitudes computed over the last 65 ka, using output maps from the MMD viscoelastic sea level model. All simulations spanning the Heinrich events and extending to ~ 7 ka predict LS M_2 amplitudes in the range 2.5–3.7 m, much larger than the present-day value of 1.5 m (the latter shown as a horizontal green line). We performed five iterations of the SAL term (four beyond the scalar approximation) for each simulation. Figure 5 plots the mean and standard deviation (the latter indicated by error bars) of iterations three, four, and five. In Figure 1b of AMMM we plotted amplitudes from the third iteration (which gave LS amplitudes in the range of 2.7–3.9 m). In a select few simulations, AMMM performed more than three iterations, and we found that the LS M_2 amplitude can vary by up to 0.6 m between iterations. We therefore took 0.6 m as a rough error estimate for the predicted paleotidal amplitudes. The 0.6 m value now appears to be an overestimate of the error due to the “jiggle” in the iterations of the SAL term. However, there are other sources of error, for instance, sensitivities to uncertainties in the sea level models or to different assump-

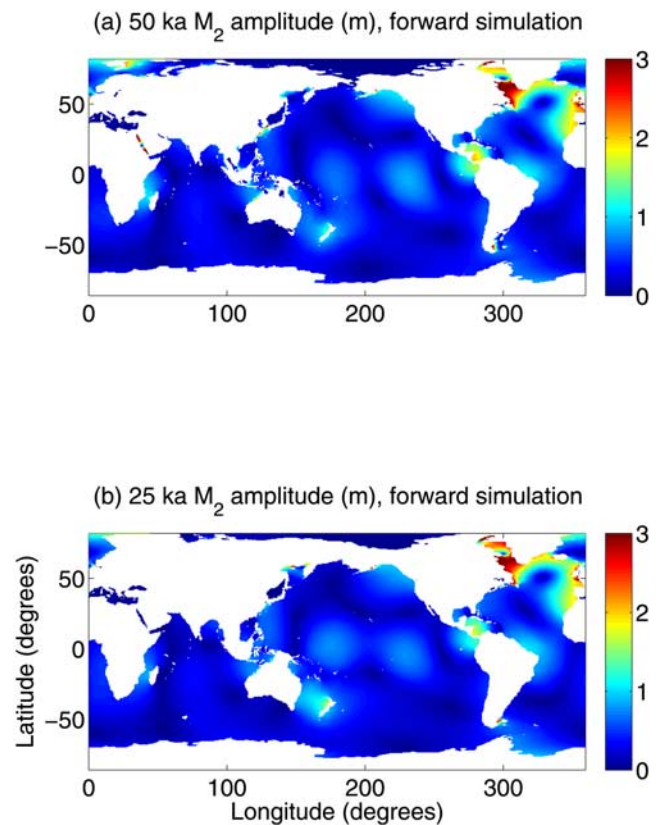


Figure 3. Global maps of M_2 amplitude (m) in $1/2^\circ$: (a) 50 ka and (b) 25 ka forward simulations utilizing spatially varying sea level maps from MMD sea level model.

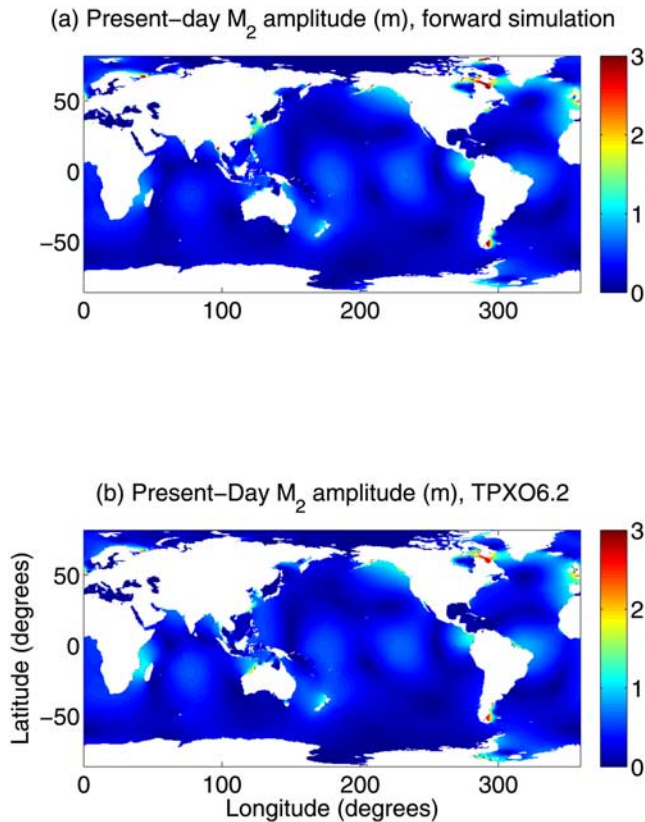


Figure 4. Global maps of M_2 amplitude (m) in (a) $1/2^\circ$ present-day forward simulation and (b) TPXO6.2 satellite altimetry constrained model [Egbert *et al.*, 1994] of present day.

tions about the paleo abyssal stratification. These other sources of error will be discussed in more detail shortly. For now we note that the uncertainties in the tide and sea level models are too large to associate much significance to the peaks and troughs lying on top of the more robust elevated glacial signal in our Figure 5.

4.3. Results of Ocean Tide Model Forced by Spatially Uniform Reductions in Sea Level

[21] For the purposes of comparison, we also show in Figure 5 (blue and magenta curves) the LS M_2 amplitudes in simulations in which eustatic and Red Sea sea levels (blue and magenta curves, Figure 2) are adopted in a spatially uniform manner to infer paleobathymetries, and in which the ocean/land ice mask used in the viscoelastic model is not utilized. We performed simulations with selected uniform sea level drops, of 10, 20, 30, 40, 60, 80, 100, and 130 m, after which a spline was used to fit the M_2 amplitudes to the eustatic and Red Sea sea level values corresponding to the horizontal axis in Figure 5 (and given in the vertical axis of Figure 2). In cases where the Red Sea sea level values are slightly above those of the present day, we took the value of the tide to equal that of the present day. Again, means and standard deviations over iterations three, four, and five of the SAL term are shown. Using the eustatic and Red Sea sea level values, we predict LS M_2 tides larger than those of

today, but less than those predicted from usage of the spatially varying sea level model. The tides computed from the eustatic sea level values approach those computed from the spatially varying sea level model only over a limited time window, close to the LGM. The tides computed using Red Sea values are somewhat smaller than those using the eustatic values, because the maximum drop in the Red Sea values over the last 65 ka is not as large as that in the eustatic curve. The simulations with spatially uniform sea level reductions will prove useful when we examine the factors behind the large LS paleotides.

4.4. Factors Behind Large Labrador Sea Paleotides

[22] The question arises: What characteristic of the ice age ocean leads to an amplification of LS tides? The tidal amplitudes do not appear to be related in a simple way to either LS or eustatic sea level. Simulations prior to 7 ka have both large LS tides and significant LS sea level drops relative to the present (~ -40 m or lower). However, the 6 ka simulation, with an LS relative sea level of ~ -80 m, did not yield a large LS tide. Eustatic sea level in the 7 ka simulation was only 7.6 m lower than present, but the 7 ka LS M_2 amplitude is nearly as large as in simulations with much lower eustatic sea level. Eustatic sea level during the interval spanning the H4–H6 events (for example) was at least ~ 50 m lower than at present, but LS M_2 tides predicted under the assumption of eustasy (blue curve, Figure 5) are relatively small during each of these events.

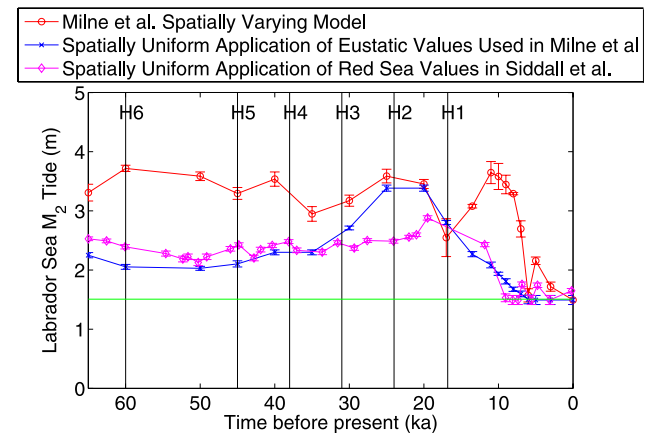


Figure 5. Labrador Sea (61.5°N , 296°E) (red curve) M_2 amplitude (m) versus time in $1/2^\circ$ forward tide model utilizing relative sea level and ocean/land ice mask predictions from spatially varying MMD sea level model. Labrador Sea (blue curve) M_2 amplitude versus time in $1/2^\circ$ forward tide model utilizing eustatic relative sea level (Figure 2, blue curve) applied in a spatially uniform manner and in which the ocean/land ice mask used in the viscoelastic sea level model is not employed. Labrador Sea (magenta curve) M_2 amplitude versus time in $1/2^\circ$ forward tide model utilizing Red Sea sea level (Figure 2, magenta curve) [Siddall *et al.*, 2006] similarly applied in a spatially uniform manner. Present-day Labrador Sea (green line) M_2 amplitude in TPXO6.2 [Egbert *et al.*, 1994]. Error bars represent only errors due to “jiggle” in the iterations of the self-attraction and loading term.

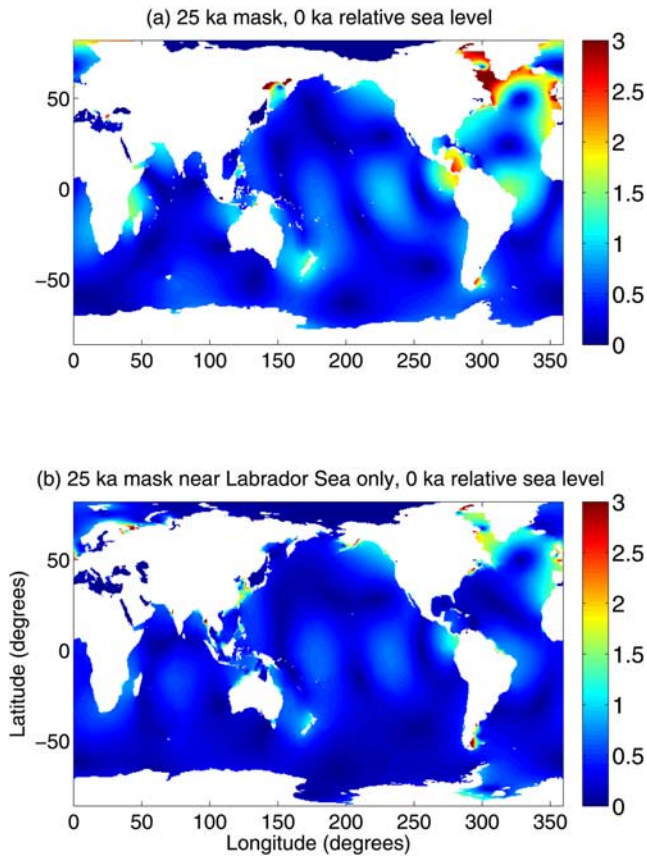


Figure 6. Global maps of M_2 amplitude (m) in $1/2^\circ$ simulations with (a) 25 ka ocean/land ice mask from MMD model and (b) 25 ka ocean/land ice mask applied only in Labrador Sea region. In both simulations, present-day water column thicknesses are used in remaining oceanic grid points.

[23] A possibility which we explore in Figure 6 is that changes in ocean basin geometry play a key role in determining LS tidal elevations. Figure 6a shows the M_2 amplitude in a simulation in which we adopt the same ocean/land ice mask used in the 25 ka simulation of Figure 3b, but in which water column depths in the remaining ocean grid points are unchanged from present-day values. Differences between Figure 3b and 6a are seen, for instance, in the Caribbean, the equatorial Pacific, the Indian Ocean between Africa and Madagascar, and the Sea of Okhotsk. These differences indicate that changes in water column thickness do impact the tides. However, changes in water column thickness do not seem to be of first-order importance in explaining the large LS paleotides. The magnitude and spatial pattern of tidal amplitudes in the LS region in the hybrid calculation (Figure 6a) is markedly similar to that in the 25 ka simulation (Figure 3b). On the basis of the hybrid calculation, we suggested in AMMM that the primary control on LS tides involved changes in the basin geometry, not changes in water column thickness. We further noted there that in simulations prior to 7 ka, our ocean/land ice mask is characterized by an ice covered Hudson Bay. We

implied that this particular change in basin geometry (blocking Hudson Strait) is an important control on the LS tides. However, our subsequent calculations indicate that the story is more complex.

[24] Figure 6b demonstrates that changes in the local geometry of the LS region can only explain part of the increase in LS tides. Figure 6b shows the M_2 amplitude map in a simulation in which the 25 ka mask is applied only in a region around the LS, specifically, inside the box bounded by 239.5°E and 324.5°E in longitude, and by 48.5°N and 82°N in latitude. Once again, water column thicknesses in the remaining oceanic grid points are unchanged from present-day values. In this simulation, LS tidal amplitudes are significantly enhanced over those in the present day (compare to Figure 4), but not by as much as they are in ice age conditions (or with the ice age ocean/land ice mask, taken together with unaltered water column thicknesses, as in Figure 6a). In a study of the present-day tides of the LS region, *Arbic et al.* [2007] performed a simulation with present-day geometry, but with a closed Hudson Strait. This change in basin geometry led to an increased LS tide, consistent with the suggestion of AMMM regarding the importance of Hudson Strait. *Uehara et al.* [2006] also conclude that closing off Hudson Strait enhances North Atlantic tides. However, as in the simulation shown in Figure 6b, the LS tide in the blocked Hudson Strait simulation of *Arbic et al.* [2007] is not as large as in simulations under full ice age conditions, or as in the simulation shown in Figure 6a. The closing off of Hudson Strait is an important part of the control local geometry has on LS tides, but local geometry is apparently only one factor behind large LS paleotides.

[25] Our next simulation demonstrates the importance of changes outside of the LS region for the LS tides. Figure 7a shows the M_2 amplitude in a simulation in which the 25 ka ocean/land ice mask is applied everywhere except in the LS region, that is, everywhere outside of the box defined above. Again, water column thicknesses in oceanic grid points are unaltered from present-day values. The result is an enhanced LS tide, larger than in Figure 6b (with changes to local geometry only), but still smaller than in Figure 6a (25 ka ocean/land ice mask) or in the 25 ka simulation (Figure 3b). The simulation shown in Figure 7a indicates that conditions outside of the LS region also affect LS tides, and that enhancement of the LS tide can take place even when the Hudson Strait remains open.

[26] The simulations done with spatially uniform drops in sea level (blue and magenta curves, Figure 5) further demonstrate that large LS tides can arise with an open Hudson Strait. These simulations are all characterized by an open Hudson Strait, since they adopt the present-day ocean/land ice mask (although changes in the geometry of the Hudson Bay region are accounted for as sea level rises and falls). Large LS tides nonetheless arise in simulations with a large uniform sea level drop. Figure 7b shows the M_2 amplitude in the simulation with a uniform sea level drop of 130 m. The size and spatial pattern of the tidal amplitudes in the LS region is very similar to that seen in the ice age simulations (prior to 7 ka) or in the simulation shown in Figure 6a (25 ka ocean/land ice mask). The 5 ka simulation

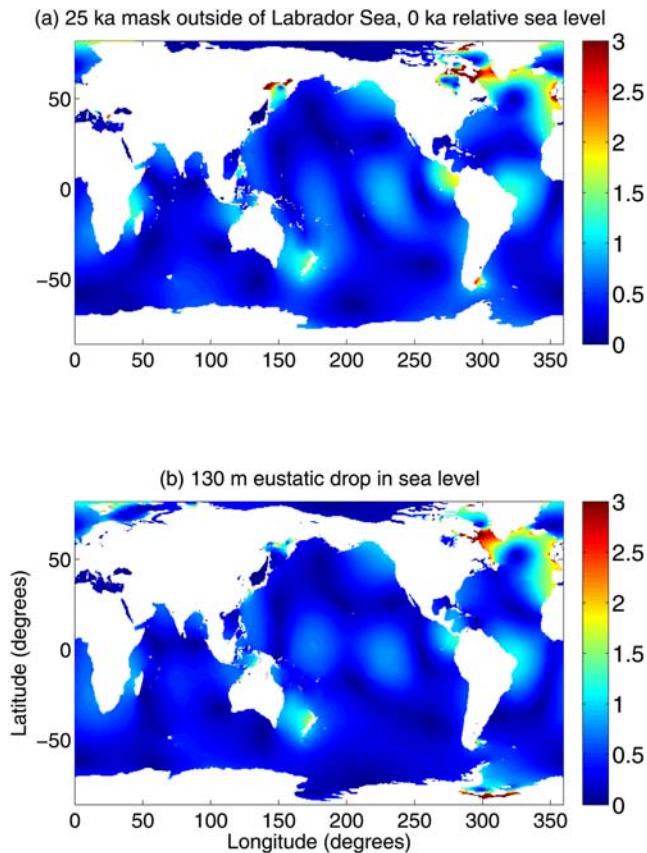


Figure 7. Global maps of M_2 amplitude (m) in (a) $1/2^\circ$ simulation with 25 ka ocean/land ice mask from MMD model applied everywhere except in Labrador Sea region and present-day water column thicknesses utilized in all oceanic grid points and (b) $1/2^\circ$ simulation with a spatially uniform drop of 130 m in sea level and in which the ocean basin geometry is not influenced by changes in the geometry of the ice model used in MMD.

(not shown) also displays significantly enhanced LS tides, despite an open Hudson Strait.

[27] Table 1 lists the M_2 elevation amplitude (m) at our nominal LS location (61.5°N , 296°E) and at a North Atlantic location just outside (50°N , 310°E) of the Labrador Sea, in the simulations described in this subsection. We also list selected other simulations that help us to understand the factors behind the large LS paleotides. Under present-day conditions, the tide in the Labrador Sea is ~ 1.5 m, in both TPXO6.2 and in our forward model (first two lines of Table 1), while the tide just outside of the Labrador Sea is rather small (0.23 m in TPXO6.2, 0.38 m in the forward model). Blocking the Hudson Strait [Arbic *et al.*, 2007] (line 3 in Table 1) enhances both the LS and outside tides considerably, as does applying the 25 ka ocean/land ice mask near the Labrador Sea only (line 4 of Table 1). Application of the 25 ka mask everywhere outside of the Labrador Sea also enhances both the LS and outside tides (line 5 of Table 1). However, none of these first 5 simulations listed in Table 1 show enhancement in the LS and

outside tides as large as that seen in the last 4 simulations listed, which are run with full (or nearly full) ice age conditions, e.g., 25 ka mask used everywhere (but with no changes in water column thickness, line 6 of Table 1), the 25 ka and 50 ka simulations (lines 7 and 8), and the simulation with a spatially uniform sea level drop of 130 m (line 9). Again, we see that both local and nonlocal changes to basin geometry contribute to the large LS paleotides. For both local and nonlocal changes, it is difficult to separate out in these simulations whether it is changes to tidal resonances, or a reduction in areas of high dissipation along shelves, that leads to increased LS tides. Even a change in basin geometry as simple as blocking Hudson Strait reduces (indeed, omits) an area of high dissipation (Hudson Strait and Bay) at the same time that resonances are altered. Table 1 demonstrates another point, one that can also be seen by visually inspecting the figures referenced in its second column. Namely, both the LS and outside tides are affected by changes in geometry, whether the changes are local to the LS, or outside of the LS.

[28] Some further progress in understanding our simulations can be obtained with “back-of-the-envelope” reasoning. The natural, or resonant, period of an ocean basin scales as L/\sqrt{gH} , where L is the horizontal length scale of the basin, and H is the basin depth. In the open ocean, where H is typically 4000 m, changes in water column thickness of order 100 m, as took place during the last ice age, bring about only a $\sim 1\%$ change in \sqrt{gH} , the phase speed of the tide. Inspection of the present-day versus 25 ka topography across the North Atlantic along lines of 51°N and 27°N reveals that fractional changes in the horizontal scale of the deep ocean are even smaller. Thus changes in the basin geometry and water column thickness of the deep ocean

Table 1. Amplitude of M_2 Tidal Elevations in the Labrador Sea and in the North Atlantic Just Outside of the Labrador Sea^a

Description	Figure	LS Amplitude (m)	Outside Amplitude (m)
TPXO6.2	4b	1.51	0.23
Present-day, forward model	4a	1.56	0.38
Hudson Strait blocked [Arbic <i>et al.</i> , 2007]	3c	2.28	0.92
25-ka mask used only near LS	6b	1.96	1.04
25-ka mask used outside of LS	7a	2.92	0.76
25-ka mask used everywhere	6a	3.77	2.00
25 ka	3b	3.47	1.64
50 ka	3a	3.53	1.71
Spatially uniform sea level drop of 130 m	7b	3.53	1.17

^aLabrador Sea (LS) location, 61.5°N , 296°E ; outside location, 50°N , 310°E . In $1/2^\circ$ simulations intended to shed light on the local and nonlocal factors lying behind large Labrador Sea paleotides. Simulations are referred to by a brief description and by the figure that displays the simulation. All results taken from our forward tide model, except for “TPXO6.2,” a highly accurate satellite-constrained tide model. All forward model results taken from the third iteration of the self-attraction and loading (SAL) term. “Hudson Strait blocked” simulation is displayed by Arbic *et al.* [2007, Figure 3c].

appear to be of little importance. On the other hand, the dissipation changes to first order between the present and the ice ages [Egbert *et al.*, 2004]. The depths and horizontal scales of the shelves do as well. We tentatively conclude that changes in the dissipation (both in deep water and on shelves) and in coastal geometries are likely to lie behind the large LS paleotides.

[29] Our results on the importance of nonlocal changes to basin geometry on the LS tides are qualitatively consistent with results obtained by Uehara *et al.* [2006] by very different methods. They compared a high-resolution ($1/12^\circ$) regional model of the northwest European shelf driven by boundary forcing from present-day tides, to the same shelf model driven by boundary forcing from a $1/2^\circ$ global paleotide model similar to ours. Prior to 10 ka, the shelf tides were substantially larger when forced by the paleotide model. Uehara *et al.* [2006] concluded that a major driver of changes in the shelf tide is changes in the open-ocean tides forcing the shelf. Our simulations also demonstrate that conditions outside the LS are important to the tides inside the LS, and additionally that the outside tide is influenced by conditions inside the LS.

4.5. Paleotide Model Sensitivity to Other Changes in Geometry

[30] In our 17 ka simulation, the tide on the European coastline is large near the artificial northern boundary along 82°N . This large European tide reduces dramatically when the artificial boundary is moved farther north, to 86°N . This reduction in the large European tides, together with the fact that the large European tide is not present in our simulations for times other than 17 ka, leads us to regard it as a numerical artifact rather than a robust result. We also ran the 20 ka and 45 ka simulations with the artificial northern boundary at 86°N rather than 82°N . In both cases, as in the 17 ka case, we found little difference in the LS M_2 amplitudes, indicating that the artificial northern boundary is of little consequence to the results on LS tides we focus on in this article.

[31] Tides in the present-day Nares Strait (west of Greenland) are much larger in our forward model than in accurate satellite-constrained models (see Figure 4). A new tide model being developed by the first author and collaborators at the Naval Research Laboratory (NRL) has a present-day Nares Strait M_2 tide that is much reduced from that in the AGHS model. Since the NRL model is truly global, whereas the AGHS model has an artificial northern boundary at 82°N , we conclude that this artificial boundary is probably the cause of the large Nares Strait tides in the AGHS model. To ensure that the (apparently) artificially large Nares Strait tide does not unduly influence simulated LS paleotides, we performed a 45 ka simulation in which the Nares Strait is filled in, and a 45 ka simulation in which the northern boundary is moved to 86°N and the Nares Strait is carved out all the way to this boundary. In both cases, the predicted 45 ka LS tide is little different from its value in the nominal 45 ka simulation.

[32] We performed a 45 ka simulation in which the water column depth over the area thought to be covered by the fringing LS ice shelf [Hulbe *et al.*, 2004] was reduced by

300 m, an assumed ice shelf thickness. The LS M_2 tidal amplitude was altered by only 0.3 m. This simulation also demonstrates that the paleotide model results are unlikely to be affected by the thickness of the Heinrich sediments themselves, since these thicknesses, while substantial, are much less than 300 m even near the Hudson Strait [e.g., Dowdeswell *et al.*, 1995].

4.6. Paleotide Model Sensitivity to Abyssal Stratification

[33] As noted earlier, paleotide models are sensitive to the poorly known paleo abyssal stratification. The deep ocean was denser during the LGM than it is today [Adkins *et al.*, 2002]. However, this inference does not by itself provide firm information about abyssal N values, which are defined as vertical derivatives of the density near the bottom, normalized by the density itself. As done by AMMM, and Egbert *et al.* [2004], we opt to perform sensitivity tests to investigate this potentially important uncertainty. We performed $1/2^\circ$ 45 ka simulations in which the strength of the optimally tuned present-day topographic drag was adjusted by factors, ranging from $1/4$ to 4 , everywhere in the model domain. In the terminology of AGHS, we adjusted the multiplicative factor from 1.75 ($1/4$ of the optimal value of 7 for present-day $1/2^\circ$ simulations) to 28 (4 times the optimal value). In the simulations with $1/4$ and $1/2$ present-day drag, LS M_2 amplitudes are nearly equal to those in the 45 ka simulation with present-day topographic drag. In simulations with $2\times$ and $4\times$ present-day drag, the amplitude decreases by 20 and 45 percent, respectively, from the amplitude computed assuming present-day drag. Global amplitude maps (Figure 8) demonstrate that in the simulations with $2\times$ and $4\times$ present-day drag, the LS paleotides are still larger than those in most other locations. Thus, regardless of the global mean tidal amplitude, the glacial LS tides were evidently anomalously large. Furthermore, because bottom waters in the glacial ocean were likely to have been well mixed by large abyssal tidal dissipations [Egbert *et al.*, 2004], we believe that an abyssal drag much larger than that of the present day is unlikely. Since N is proportional to the square root of the vertical derivative of density, this derivative would have to have been 16 times larger in the ice ages than it is today for the $4\times$ present-day drag scenario to apply, a very severe assumption.

[34] One could make a very rough estimate of abyssal N values during the LGM by assuming that horizontal variations in density are mapped onto vertical variations by the oceanic circulation (D. Sigman, personal communication, 2004). We examine bottom water densities at the four Ocean Drilling Program (ODP) sites listed by Adkins *et al.* [2002, Table 1] for this purpose. We reference potential density to 3436 db, which is the pressure in the modern-day ocean corresponding to the latitude of site 981 and a depth of 3384 m (the average depth of ODP sites 1063 and 981). We compute potential densities for the modern and LGM ocean at the four ODP sites using the potential temperatures and salinities listed in Adkins *et al.* [2002, Table 1]. We find that the differences in density between their two Southern Hemisphere sites were larger by a factor of 6.4, during the LGM, while the differences between their two Northern

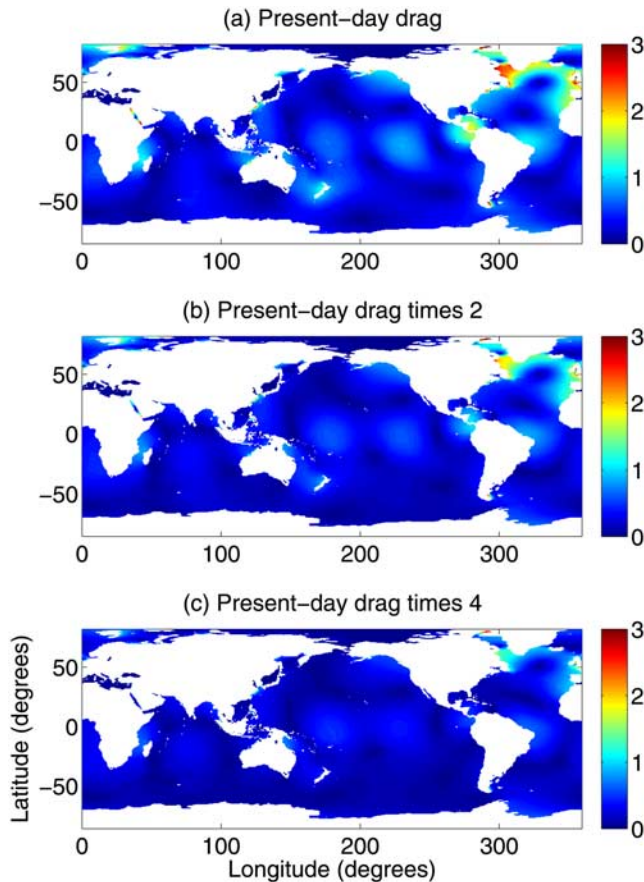


Figure 8. Global maps of M_2 amplitudes (m) in $1/2^\circ$ 45-ka simulations utilizing MMD spatially varying sea level model with (a) present-day topographic wave drag assumed, (b) $2\times$ present-day topographic drag, and (c) $4\times$ present-day topographic drag.

Hemisphere sites were smaller by a factor of 0.4. We then estimate that Southern Hemisphere N values during glacial times may have been larger by $\sqrt{6.4} = 2.5$ than those of the present day, while Northern Hemisphere N values may have decreased. Thus, abyssal N values may have been about twice as large as those of today, in a global average. In this case, the simulations discussed above indicate that large LS paleotides would have prevailed.

[35] Another note on the issue of abyssal stratification is that parameterizations of topographic wave drag employed in atmospheric models [e.g., Garner, 2005] employ both terms which are linear in the flow (in which the drag also depends on N) and terms which are quadratic in the flow (in which the drag formula itself does not depend on N , though conditions for nonlinearity do). At present, ocean tide models employ only the linear topographic drag terms. However, as our knowledge of topographic drag in the ocean increases it is at least possible that the nonlinear term will be seen to be more important, in which case the concerns above regarding abyssal stratification would take on less importance.

4.7. Paleotide Model Simulations at Higher Horizontal Resolution

[36] To test the effect of horizontal resolution on the tide model results, we first ran the 17 ka and 45 ka simulations at $1/4^\circ$ horizontal resolution, in addition to the nominal $1/2^\circ$ resolution used in the majority of our simulations. The LS tidal amplitude, as well as the jitter from iteration to iteration of the SAL term, are little affected by this increase in resolution. To further address the impact of resolution, we performed a limited number of $1/8^\circ$ simulations. Consistent with Egbert *et al.* [2004], we found that our present-day $1/8^\circ$ M_2 solution is considerably improved over the lower-resolution simulations. (For reasons discussed in AGHS, we were able to obtain the same tidal elevation accuracy in our $1/2^\circ$ solutions as in our $1/4^\circ$ solutions, though at the expense of increased subgrid-scale noise in the $1/2^\circ$ case. The $1/8^\circ$ solutions are improved over both the $1/2^\circ$ and $1/4^\circ$ solutions.) Part of the improvement in the $1/8^\circ$ solutions arises from employment of the topographic drag in coastal areas as well as in the deep ocean (i.e., in all waters deeper than 100 m, not just in waters deeper than 1000 m). When compared to the $1/2^\circ$ (or $1/4^\circ$) solutions, our $1/8^\circ$ solution has a lower sea surface elevation error (5.34 cm versus 7.76 cm) with respect to satellite altimeter observations of the present-day M_2 tide. Thus 96% of the M_2 variance in satellite altimeter records is captured rather than 92%. The $1/8^\circ$ solution has a lower fraction of the tidal dissipation occurring in waters deeper than 1000 m than does the $1/2^\circ$ solution ($1/3$ rather than $1/2$; again, this is due in part to the employment of topographic drag in coastal waters). The shelf/deep-ocean partition of tidal dissipation in the present-day $1/8^\circ$ solution is more in line with that seen in the Egbert and Ray [2003] observational study, as well as in other forward tide model studies [e.g., Jayne and St. Laurent, 2001; Egbert *et al.*, 2004]. Finally, our $1/8^\circ$ solution achieves these more accurate elevations and spatial distributions of tidal dissipation with a smaller multiplicative factor (optimal value of 4). We find that LS M_2 amplitudes in $1/8^\circ$ 45 ka simulations with present-day drag (multiplicative factor of 4) are comparable to those found in the $1/2^\circ$ simulations reported on earlier. Thus our $1/2^\circ$ horizontal resolution simulations appear to be adequate for the purposes of this article.

4.8. Multiconstituent Paleotide Simulations

[37] We performed two $1/2^\circ$ 45 ka multiconstituent simulations, one with present-day drag and one with $4\times$ present-day drag. Because multiconstituent simulations are more computationally expensive than M_2 -only runs, we only iterated the multiconstituent simulations once past the scalar approximation. Maps of the S_2 , N_2 , and K_2 amplitudes (not shown) also feature anomalously large values in the LS, while K_1 , O_1 , P_1 , and Q_1 , as in the present day, are rather small in the LS. For both values of drag, the maximum LS peak-to-peak tidal range (spring tide) is about 3.5 times larger than the LS M_2 tidal amplitude. If we multiply the LS M_2 amplitudes in Figure 5 by 3.5, we conclude that, under the assumption of an abyssal stratification about equal to that of today, the peak-to-peak amplitude of the LS spring paleotide is about 9–13 m (prior

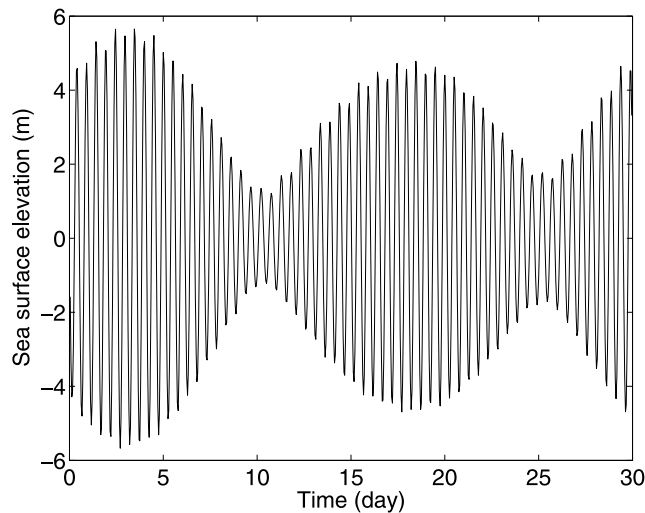


Figure 9. Forward-modeled Labrador Sea (61.5°N, 296°E) tidal elevations (m) over a typical 30-day period in 1/2° 45-ka multiconstituent simulation with present-day topographic wave drag assumed and utilizing spatially varying MMD sea level model.

to 7 ka). These are comparable to the largest spring tidal ranges in the present-day ocean, in Hudson Strait and the Bay of Fundy, which can reach up to 17 m. Furthermore, the large LS paleotides occurred over a much greater areal extent. Figure 9 shows the sea surface elevation at our nominal LS grid point (61.5°N, 296°E) during a typical 30-day period in the 45 ka present-day drag multiconstituent simulation. The spring and neap tides are easily discernible.

5. Comparison to Other Paleotide Studies and Sensitivity to Adopted Sea Level Model

[38] Examination of the M_2 amplitude maps of *Uehara et al.* [2006], who focused on paleotides of the northwest European shelf; *Egbert et al.* [2004]; and *Griffiths and Peltier* [2008, also submitted manuscript, 2008] also reveals a local maximum value in the paleo LS, of about 3 m. Note that all four of these studies focus on the LGM and post-LGM ocean. As noted by *Uehara et al.* [2006], there are quantitative differences between the results in different studies, which they suggest are likely due to discrepancies between the adopted sea level models. *Uehara et al.* [2006] demonstrated the paleotide model sensitivity to sea level model by showing that the timing of the drop from large amplitude ice age tides to the lower-amplitude tides of modern times on the northwest European shelf depends on the specific sea level model adopted. Their LS tides (K. Uehara, personal communication, 2007) do not show troughs at 17 ka and 6 ka, nor a peak near 10 ka, as ours do.

[39] We followed up the suggestion of *Uehara et al.* [2006] on the importance of the adopted sea level model by performing 1/2° 10 ka and 20 ka M_2 simulations with the ICE-5G sea level model [*Peltier*, 2004], an updated version of the *Peltier* [1994] model used by *Uehara et al.* [2006]. We will compare the results with those using the MMD sea level model adopted in most of our simulations. Table 2 lists

the LS M_2 elevations computed from our tide model using the two different sea level models, as well as the elevations in *Uehara et al.* [2006; K. Uehara, personal communication, 2007]. For our tide model, we show both results obtained with the scalar approximation for SAL, and results obtained with an iterative procedure for SAL (note that *Uehara et al.* [2006] used the scalar approximation only, not the full iterative procedure). We also show both results of simulations with topographic drag acting over all locations with seafloor depths exceeding 1000 m (and a multiplicative factor of 7), and results of simulations with drag acting over all locations having a seafloor depth exceeding 100 m (and a multiplicative factor of 5). We find, as did *Uehara et al.* [2006], that the choice of sea level model affects the paleotide model results. A study of Table 2 shows that the *Peltier* [1994, 2004] sea level models always lead to substantially larger LS tidal elevations at 20 ka than at 10 ka. There is a significant decrease in LS tidal amplitude from 20 ka to 10 ka when the MMD sea level model and the scalar approximation are used. However, there is no significant difference between LS elevations at 10 ka and 20 ka in simulations using the MMD sea level model and an iterative SAL. Table 2 lends support to the hypothesis of *Uehara et al.* [2006] that the quantitative inconsistencies between their results and the AMMM results are due to the different sea level models adopted. Finally, we note that differences between the LS paleotides in simulations with topographic drag acting over all waters deeper than 1000 m (and a multiplicative factor of 7) on the one hand, and those in simulations with topographic drag acting over all waters

Table 2. Amplitude of M_2 Tidal Elevations in the LS (61.5°N, 296°E) at 20 ka and 10 ka^a

Epoch	Tide Model	Sea Level Model	SAL	Amplitude (m)
10 ka	USHLP	P94	scalar	2.50
20 ka	USHLP	P94	scalar	4.21
10 ka	AGHS2	P04	scalar	3.09
20 ka	AGHS2	P04	scalar	4.11
10 ka	AGHS2	P04	iterative	3.20 ± 0.06
20 ka	AGHS2	P04	iterative	4.72 ± 0.29
10 ka	AGHS1	P04	scalar	2.87
20 ka	AGHS1	P04	scalar	3.79
10 ka	AGHS1	P04	iterative	2.98 ± 0.05
20 ka	AGHS1	P04	iterative	4.32 ± 0.21
10 ka	AGHS2	MMD	scalar	3.26
20 ka	AGHS2	MMD	scalar	4.90
10 ka	AGHS2	MMD	iterative	3.80 ± 0.23
20 ka	AGHS2	MMD	iterative	3.73 ± 0.14
10 ka	AGHS1	MMD	scalar	3.05
20 ka	AGHS1	MMD	scalar	4.45
10 ka	AGHS1	MMD	iterative	3.58 ± 0.22
20 ka	AGHS1	MMD	iterative	3.45 ± 0.08

^a“USHLP” denotes results from *Uehara et al.* [2006], who use the *Peltier* [1994] (P94) sea level model and the scalar approximation for SAL. “AGHS1” denotes results from our 1/2° tide model, with multiplicative factor of 7 and topographic drag utilized in all waters deeper than 1000 m. “AGHS2” denotes results from our 1/2° tide model, with multiplicative factor of 5 and topographic drag utilized in all waters deeper than 100 m. Sea level models used in the AGHS simulations are *Milne et al.* [1999] (MMD) and ICE-5G [*Peltier*, 2004] (P04). For AGHS simulations, results are shown for both the scalar approximation to SAL and for iterative solutions (average of iterations 3–5 shown for the latter; error bars indicate one standard deviation).

deeper than 100 m (and a multiplicative factor of 5) on the other hand, are small.

6. Summary and Discussion

6.1. Summary of Paleotide Results

[40] We have investigated tidal elevations over the last 65 ka using a forward tide model that captures 92% of the present-day open-ocean tidal elevation variance, in conjunction with a sea level model [MMD] that offers estimates of the ocean/land ice boundary as well as spatial variations in relative sea level. Under the assumption of an abyssal topographic wave drag equal in strength to that of the present day, our simulations yield Labrador Sea (LS) M_2 elevation amplitudes of 2.5–3.7 m (5.0–7.4 m peak-to-peak) over a wide time window encompassing the Heinrich events H1–H6. We estimate that LS spring tides reached peak-to-peak values of about 9–13 m over the same time interval, comparable to the largest spring tidal ranges in the present-day ocean. Uncertainties in paleotide estimates arise from uncertainties in tide models, in sea level models, in knowledge of abyssal stratification (which enters into topographic wave drag), and from jitter in iterations of the self-attraction and loading term. These uncertainties, though substantial, do not significantly reduce the likelihood that tides in the glacial LS were much larger than those in all but a few locations of either the present-day or ice age ocean.

[41] We have demonstrated that LS tidal amplitudes are strongly affected by changes in both local geometry (i.e., changes in the ice cover over Hudson Bay and Strait), and in geometries outside of the LS region. It is difficult to separate out whether geometry changes (whether local or nonlocal) affect tides because of changes in the resonance of basins or because the areal extent of continental shelves, which dissipate much of the tidal energy, is reduced with lower sea levels. Some progress in attaining this separation may be made if computations of the normal modes [e.g., Platzman *et al.*, 1981] are performed for ice age conditions, to determine whether tidal resonances changed substantially with changes in basin geometries.

6.2. Potential Implications for Heinrich Events

[42] There is a growing body of evidence from observations in present-day Antarctica of the impacts of tidal mechanical forcing on both continental ice streams and floating ice shelves [e.g., Murray *et al.*, 2007, and references therein]. Motivated by this evidence, we postulate that large tidal elevations in the glacial LS may have played a catalytic role in ice age ice sheet dynamics, in particular, in the formation of Heinrich events. At the very least, the large LS paleotides are an important boundary condition that should enter discussions of Heinrich event mechanisms. Ice age paleotides in Europe were of comparable size to those in the LS only near the British Isles. The strong glacial LS tides may explain in part why Canadian detritus is more prominent than European detritus in Heinrich event sediments, although the larger size of the ice streams in Labrador must also be a factor. If our hypothesis of a tidal role in Heinrich events is correct, then the large LS paleotidal elevations associated with ice age conditions represent a negative feedback on the stability of the Lau-

rentide ice sheet, and a potentially important link with millennial-scale ice age climate change.

[43] Our hypothesis of a tidal role in Heinrich events differs from previous hypotheses of a tidal role in millennial-scale climate variability [e.g., Keeling and Whorf, 1997, 2000] in two important ways. First, we possess a forward model of the tides, which we can use to estimate global patterns of the tidal response to astronomical tidal forcing and to identify regions of especially large response. Keeling and Whorf [1997, 2000] discussed long-period modulations in the tidal forcing, without any model of the tidal response or its geographic variability. Second, Keeling and Whorf [1997, 2000] proposed that variations in tidal mixing (arising from the variations in forcing) lead to climate variability, through their influence on sea surface temperatures. Egbert *et al.* [2004, Figure 9] have shown that mixing was indeed large in the paleo LS. Thus, tidal mixing may have played a role in ice sheet dynamics during glacial times. We have noted here that large tidal elevations in the LS provide substantial mechanical forcing on ice sheets and shelves. The impact of tidal mechanical forcing on ice sheets and shelves has received less attention than the impact of tides on ocean mixing, in the recent (fairly voluminous) literature discussing the role of tides in climate.

[44] The binge-purge hypothesis of MacAyeal [1993] provides an explanation for the ~7000-year intervals between Heinrich events, but does not explain why the Hudson Strait ice stream in particular was the dominant source of episodic ice sheet instability. In contrast, the work presented here, while offering a potential explanation for the dominance of the Labrador Sea/Hudson Strait over other regions in Heinrich event formation, does not appear to provide an obvious explanation for the timings of Heinrich events. It is difficult to see a 7000-year cycle in our tide model results (Figure 5), for example. There is unquestionably some energy in long periods (e.g., periods longer than a year) in the tidal forcing. The best-known example is the lunar nodal cycle, which modulates the amplitudes of O_1 and K_1 by 18 and 11 percent, respectively, over an 18.6-year cycle. Loder and Garrett [1978] and others have argued that the nodal cycle modulates ocean mixing which in turn leads to an 18.6-year cycle in ocean temperatures. Keeling and Whorf [1997, 2000] argue that variations in tidal forcing modulate mixing and hence climate on a timescale of 1795 years. Munk *et al.* [2002] estimate the strength of tidal astronomical forcing at 1795 years at a location near Hawaii and find an amplitude of ~0.04 mm, about 3–4 orders of magnitude smaller than the astronomical forcing of, for instance, M_2 . Munk *et al.* [2002] find that the 1795-year line is the strongest line in the band between 18.6 and 20,000 years. However, due to its weakness, they consider the 1795-year line to be an unlikely candidate for explaining millennial-scale climate variability.

[45] At multimillennial periods, larger amplitude modulations exist, but they are still small. Munk and Bills [2007] find modulations in tidal forcing of the order of a few percent at 41,000-year periods. As they point out, these small changes in tidal forcing are “dwarfed” by changes in the tides arising from lower sea levels. Numerical paleotide models such as the one discussed here, and those referenced

earlier, demonstrate that tidal amplitudes can change by factors of order 2 due to sea level change. It appears that tides are much more sensitive to changes in resonance (linked to changes in ocean basin geometry) and to reduction in the area of high-dissipation regions along shelves than to changes in tidal forcing, though there are some small-amplitude millennial variations in the latter.

[46] Given that millennial variabilities in tidal forcings are of small amplitude, and given that our model results suggest that LS tides were just as large in between Heinrich events as they were during Heinrich events, we cannot conclude at present that tides can explain the time intervals between Heinrich events. We believe that large LS tides by themselves are unlikely to have been the sole trigger of Heinrich events. More likely, they may have played a “preconditioning” role for other triggers such as sea level rise or climatic warming to set off discrete Heinrich events. It is possible that tides may have acted in concert with other mechanisms. For instance, tides may have weakened ice shelves until external forcing led to a catastrophic collapse, as in the hypothesis of *Hulbe et al.* [2004]. Another possibility is that the timing of Heinrich events is set by the binge-purge mechanism of *MacAyeal* [1993], while large LS tides pinpoint the LS as the spatial location of the largest iceberg discharges.

[47] The potential role of tides in the destabilization of ice sheets during the last ice age has also been discussed in great detail by *Griffiths and Peltier* [2008, also submitted manuscript, 2008]. In contrast to our study and that of *Egbert et al.* [2004], *Griffiths and Peltier* [2008, also submitted manuscript, 2008] run their model in a truly global domain, which allows examination of paleotides in the Arctic. They find large tides in the paleo Arctic ocean, in particular, at the discharge point of the Innuitian ice stream in the Queen Elizabeth Islands of the Canadian Archipelago. They argue that their results strengthen the case for a tidal role in the destabilization of ice sheets, since the Innuitian ice stream also experienced episodic collapse. *Griffiths and Peltier* [2008, also submitted manuscript, 2008] find as well that tides in the Weddell Sea were large under glacial conditions, with the amplitude being quite sensitive to the assumed locations of ice sheet grounding lines. They argue that tidal destabilization of ice sheets may have occurred in the Southern Ocean as well. *Griffiths and Peltier* [2008, also

submitted manuscript, 2008] point out that because their modeled tides (at least, in the Arctic and Antarctic) are especially sensitive to the location of ice sheet grounding lines, tidal amplitudes in these locations may have been modulated over time by the growth and decay of ice sheets.

6.3. Further Work on Paleotides and Their Potential Relation to Heinrich Events

[48] One potential improvement to paleotide studies would be to form estimates of topographic wave drag based on abyssal stratifications N taken from models of the paleoceanographic circulation, rather than on multiplications of the present-day topographic wave drag by spatially uniform factors. The former approach has been adopted by *Griffiths and Peltier* [2008, also submitted manuscript, 2008], based on the simulations of *Peltier and Solheim* [2004]. They find a slight reduction in N during the LGM, which further suggests that changes in N during the LGM were unlikely to have been large enough to strongly affect the results of the paleotide simulations presented here and in other recent articles.

[49] To investigate the potential role of tides in Heinrich events more thoroughly, quantitative models of the response of ice sheets to tides must be developed. The glaciological community is currently developing such models for particular ice streams in Antarctica [e.g., *Bindschadler et al.*, 2003], but the authors are not aware of any models of tidal effects on continental-scale ice sheets, for either present-day or ice age conditions.

[50] **Acknowledgments.** The reviewer (Sidney Hemming) and editor (Elco Rohling) are thanked for useful comments on the manuscript. B.K.A. thanks Tim Garrett, Chris Garrett, Katsuto Uehara, Jorge Sarmiento, Anand Gnanadesikan, Walter H. F. Smith, Bob Hallberg, Samar Khattiwala, Olivier Marchal, Carl Wunsch, Harper Simmons, Mike Bender, Daniel Sigman, Ted Scambos, Sridhar Anandakrishnan, Bob Bindschadler, David Vaughan, Hilmar Gudmundsson, Andy Smith, Catherine Ritz, Sidney Hemming, Charles Jackson, Rob Scott, Dave Nolan, Stephen Griffiths, and the reviewers of AMMM for discussions related to this work. Chris Garrett provided useful suggestions on the first draft of this manuscript. B.K.A. was supported by the Carbon Mitigation Initiative of the Ford Motor Company and by National Science Foundation grants OCE-0097316, OCE-0327189, and OCE-0623159. J.X.M. thanks the Canadian Institute for Advanced Research, the National Sciences and Engineering Research Council of Canada, and the Miller Institute for Research in Basic Sciences for their support. Computations for this article were performed on the supercomputer cluster at NOAA GFDL.

References

- Adkins, J. F., K. McIntyre, and D. P. Schrag (2002), The salinity, temperature, and $\delta^{18}O$ of the glacial deep ocean, *Science*, *298*, 1769–1773.
- Alley, R. B., T. K. Dupont, B. R. Parizek, S. Anandakrishnan, D. E. Lawson, G. R. Larson, and E. B. Evenson (2006), Outburst flooding and the initiation of ice-stream surges in response to climatic cooling: A hypothesis, *Geomorphology*, *75*, 76–89.
- Anandakrishnan, S., and R. B. Alley (1997), Tidal forcing of basal seismicity of ice stream C, West Antarctica, observed far inland, *J. Geophys. Res.*, *102*, 15,183–15,196.
- Arbic, B. K., D. R. MacAyeal, J. X. Mitrovica, and G. A. Milne (2004a), Palaeoclimate: Ocean tides and Heinrich events, *Nature*, *432*, 460.
- Arbic, B. K., S. T. Garner, R. W. Hallberg, and H. L. Simmons (2004b), The accuracy of surface elevations in forward global barotropic and baroclinic tide models, *Deep Sea Res., Part II*, *51*, 3069–3101.
- Arbic, B. K., P. St-Laurent, G. Sutherland, and C. Garrett (2007), On the resonance and influence of the tides in Ungava Bay and Hudson Strait, *Geophys. Res. Lett.*, *34*, L17606, doi:10.1029/2007GL030845.
- Bard, E., F. Rostek, J.-L. Turon, and S. Gendreau (2000), Hydrological impact of Heinrich events in the subtropical northeast Atlantic, *Science*, *289*, 1321–1324.
- Bassett, S. E., G. A. Milne, J. X. Mitrovica, and P. U. Clark (2005), Ice sheet and solid earth influences on far-field sea-level histories, *Science*, *309*, 925–928.
- Bindschadler, R. A., M. A. King, R. B. Alley, S. Anandakrishnan, and L. Padman (2003), Tidally controlled stick-slip discharge of a West Antarctic ice stream, *Science*, *301*, 1087–1089.
- Bond, G., et al. (1992), Evidence for massive discharges of icebergs into the North Atlantic Ocean during the last glacial period, *Nature*, *360*, 245–249.
- Broecker, W. S., and S. Hemming (2001), Climate swings come into focus, *Science*, *294*, 2308–2309.
- Broecker, W., G. Bond, M. Klas, E. Clark, and J. McManus (1992), Origin of the northern Atlantic’s Heinrich events, *Clim. Dyn.*, *6*, 265–273.
- Brunt, K. M., L. Copland, E. B. O’Donnell, and D. R. MacAyeal (2006), Observations and

- models of tidally pulsed flow of the Ross Ice Shelf, Antarctica, *Eos Trans. AGU*, 87(52), Fall Meet. Suppl., Abstract C43B-05.
- Carrère, L., and F. Lyard (2003), Modeling the barotropic response of the global ocean to atmospheric wind and pressure forcing—Comparisons with observations, *Geophys. Res. Lett.*, 30(6), 1275, doi:10.1029/2002GL016473.
- Doake, C. S. M., R. M. Frolich, D. R. Mantripp, A. M. Smith, and D. G. Vaughan (1987), Glaciological studies on Rutford Ice Stream, *J. Geophys. Res.*, 92, 8951–8960.
- Doake, C. S. M., H. F. J. Corr, K. W. Nicholls, A. Gaffikin, A. Jenkins, W. I. Bertiger, and M. A. King (2002), Tide-induced lateral movement of Brunt Ice Shelf, Antarctica, *Geophys. Res. Lett.*, 29(8), 1226, doi:10.1029/2001GL014606.
- Dowdeswell, J. A., M. A. Maslin, J. T. Andrews, and I. N. McCave (1995), Iceberg production, debris rafting, and the extent and thickness of Heinrich layers (H-1, H-2) in North Atlantic sediments, *Geology*, 23, 301–304.
- Dziewonski, A. M., and D. L. Anderson (1981), Preliminary reference Earth model (PREM), *Phys. Earth Planet. Inter.*, 25, 297–356.
- Egbert, G. D., and R. D. Ray (2003), Semi-diurnal and diurnal tidal dissipation from TOPEX/POSEIDON altimetry, *Geophys. Res. Lett.*, 30(17), 1907, doi:10.1029/2003GL017676.
- Egbert, G. D., A. F. Bennett, and M. G. G. Foreman (1994), TOPEX/POSEIDON tides estimated using a global inverse model, *J. Geophys. Res.*, 99, 24,821–24,852.
- Egbert, G. D., R. D. Ray, and B. G. Bills (2004), Numerical modeling of the global semidiurnal tide in the present day and in the last glacial maximum, *J. Geophys. Res.*, 109, C03003, doi:10.1029/2003JC001973.
- Flückiger, J., R. Knutti, and J. W. C. White (2006), Oceanic processes as potential trigger and amplifying mechanisms for Heinrich events, *Paleoceanography*, 21, PA2014, doi:10.1029/2005PA001204.
- Garner, S. T. (2005), A topographic drag closure built on an analytical base flux, *J. Atmos. Sci.*, 62, 2302–2315.
- Griffiths, S. D., and W. R. Peltier (2008), Megatides in the Arctic Ocean under glacial conditions, *Geophys. Res. Lett.*, 35, L08605, doi:10.1029/2008GL033263.
- Grousset, F. E., L. Labeyrie, J. A. Sinko, M. Cremer, G. Bond, J. Duprat, E. Cortijo, and S. Huon (1993), Patterns of ice-rafted detritus in the glacial North Atlantic (40–55°N), *Paleoceanography*, 8, 175–192.
- Heinrich, H. (1988), Origin and consequences of cyclic ice rafting in the northeast Atlantic Ocean during the past 130,000 years, *Quat. Res.*, 29, 142–152.
- Hemming, S. R. (2004), Heinrich events: Massive late Pleistocene detritus layers of the North Atlantic and their global climate imprint, *Rev. Geophys.*, 42, RG1005, doi:10.1029/2003RG000128.
- Hendershott, M. C. (1972), The effects of solid earth deformation on global ocean tides, *Geophys. J. R. Astron. Soc.*, 29, 389–402.
- Hulbe, C. L., D. R. MacAyeal, G. H. Denton, J. Kleman, and T. V. Lowell (2004), Catastrophic ice shelf breakup as the source of Heinrich event icebergs, *Paleoceanography*, 19, PA1004, doi:10.1029/2003PA000890.
- Jayne, S. R., and L. C. St. Laurent (2001), Parameterizing tidal dissipation over rough topography, *Geophys. Res. Lett.*, 28, 811–814.
- Johnson, R. G., and S.-E. Lauritzen (1995), Hudson Bay–Hudson Strait jökulhlaups and Heinrich events: A hypothesis, *Paleogeogr. Paleoclimatol. Paleoecol.*, 117, 123–137.
- Keeling, C. D., and T. P. Whorf (1997), Possible forcing of global temperature by the oceanic tides, *Proc. Natl. Acad. Sci. U. S. A.*, 94, 8321–8328.
- Keeling, C. D., and T. P. Whorf (2000), The 1,800-year oceanic tidal cycle: A possible cause of rapid climate change, *Proc. Natl. Acad. Sci. U. S. A.*, 97, 3814–3819.
- Lambeck, K., C. Smither, and M. Ekman (1998), Tests of glacial rebound models for Fennoscandia based on instrumented sea- and lake-level records, *Geophys. J. Int.*, 135, 375–387.
- Lambeck, K., Y. Yokoyama, and T. Purcell (2002), Into and out of the Last Glacial Maximum: Sea-level change during Oxygen Isotope Stages 3 and 2, *Quat. Sci. Rev.*, 21, 343–360.
- Levitus, S., T. P. Boyer, M. E. Conkright, T. O'Brien, J. Antonov, C. Stephens, L. Stathopoulos, D. Johnson, and R. Gelfeld (1998), *World Ocean Database 1998*, vol. 1, Introduction, NOAA Atlas NESDIS 18, 346 pp., U. S. Government Printing Office, Washington, D.C.
- Loder, J. W., and C. Garrett (1978), The 18.6-year cycle of sea surface temperature in shallow-seas due to variations in tidal mixing, *J. Geophys. Res.*, 83, 1967–1970.
- Lyard, F., F. Lefevre, T. Letellier, and O. Francis (2006), Modelling the global ocean tides: Modern insights from FES2004, *Ocean Dyn.*, 56, 394–415, doi:10.1007/s10236-006-0086-x.
- MacAyeal, D. R. (1993), Binge/purge oscillations of the Laurentide Ice Sheet as a cause of the North Atlantic's Heinrich events, *Paleoceanography*, 8, 775–784.
- MacAyeal, D. R., et al. (2006), Transoceanic wave propagation links iceberg calving margins of Antarctica with storms in tropics and Northern Hemisphere, *Geophys. Res. Lett.*, 33, L17502, doi:10.1029/2006GL027235.
- Manabe, S., and R. J. Stouffer (1995), Simulation of abrupt climate change induced by freshwater input to the North Atlantic Ocean, *Nature*, 378, 165–167.
- Milne, G. A., J. X. Mitrovica, and J. L. Davis (1999), Near-field hydro-isostasy: The implementation of a revised sea-level equation, *Geophys. J. Int.*, 139, 464–482.
- Mitrovica, J. X., and A. M. Forte (1997), Radial profile of mantle viscosity: Results from the joint inversion of convection and postglacial rebound observables, *J. Geophys. Res.*, 102, 2751–2769.
- Mitrovica, J. X., and G. A. Milne (2003), On post-glacial sea level: I. General theory, *Geophys. J. Int.*, 154, 253–267.
- Moros, M., A. Kuijpers, I. Snowball, S. Lassen, D. Bäckström, F. Gingele, and J. McManus (2002), Were glacial iceberg surges in the North Atlantic triggered by climatic warming?, *Mar. Geol.*, 192, 393–417.
- Munk, W., and B. Bills (2007), Tides and the climate: Some speculations, *J. Phys. Oceanogr.*, 37, 135–147.
- Munk, W., M. Dzieciuch, and S. Jayne (2002), Millennial climate variability: Is there a tidal connection?, *J. Clim.*, 15, 370–385.
- Murray, T., A. M. Smith, M. A. King, and G. P. Weedon (2007), Ice flow modulated by tides at up to annual periods at Rutford Ice Stream, West Antarctica, *Geophys. Res. Lett.*, 34, L18503, doi:10.1029/2007GL031207.
- Peltier, W. R. (1994), Ice-age paleotopography, *Science*, 265, 195–201.
- Peltier, W. R. (2004), Global glacial isostasy and the surface of the ice-age Earth: The ICE-5G (VM2) model and GRACE, *Annu. Rev. Earth Planet. Sci.*, 32, 111–149.
- Peltier, W. R., and L. P. Solheim (2004), The climate of the Earth at Last Glacial Maximum: Statistical equilibrium state and a mode of internal variability, *Quat. Sci. Rev.*, 23, 335–357.
- Platzman, G. W., G. A. Curtis, K. S. Hansen, and R. D. Slater (1981), Normal modes of the world ocean. part II: Description of modes in the period 8 to 80 hours, *J. Phys. Oceanogr.*, 11, 579–603.
- Ray, R. D. (1998), Ocean self-attraction and loading in numerical tidal models, *Mar. Geod.*, 21, 181–192.
- Sandal, C., and D. Nof (2008), A new analytical model for Heinrich events and climate instability, *J. Phys. Oceanogr.*, 38, 451–466.
- Siddall, M., E. J. Rohling, A. Almogi-Labin, C. Hemleben, D. Meischner, I. Schmelzer, and D. A. Smeed (2003), Sea-level fluctuations during the last glacial cycle, *Nature*, 423, 853–858.
- Siddall, M., E. J. Rohling, A. Almogi-Labin, C. Hemleben, D. Meischner, I. Schmelzer, and D. A. Smeed (2006), Red Sea sea level reconstruction, *IGBP PAGES/World Data Center for Paleoclimatology Data Contribution Series 2006-063*, NOAA/NCDC Paleoclimatology Program, Boulder, Colo.
- Smith, A. M. (1991), The use of tiltmeters to study the dynamics of Antarctic ice-shelf grounding lines, *J. Glaciol.*, 37, 51–58.
- Smith, W. H. F., and D. T. Sandwell (1997), Global sea floor topography from satellite altimetry and ship depth soundings, *Science*, 277, 1956–1962.
- Thomas, M., and J. Sündermann (1999), Tides and tidal torques of the world ocean since the last glacial maximum, *J. Geophys. Res.*, 104, 3159–3183.
- Uehara, K., J. D. Scourse, K. J. Horsburgh, K. Lambeck, and A. P. Purcell (2006), Tidal evolution of the northwest European shelf seas from the Last Glacial Maximum to the present, *J. Geophys. Res.*, 111, C09025, doi:10.1029/2006JC003531.
- Williams, R. T., and E. S. Robinson (1980), The ocean tide in the southern Ross Sea, *J. Geophys. Res.*, 85, 6689–6696.
- Winton, M., and E. S. Sarachik (1993), Thermohaline oscillations induced by strong steady salinity forcing of ocean general circulation models, *J. Phys. Oceanogr.*, 23, 1389–1410.
- Wunsch, C., and R. Ferrari (2004), Vertical mixing, energy, and the general circulation of the ocean, *Annu. Rev. Fluid Mech.*, 36, 281–314.

B. K. Arbic, Institute for Geophysics, Jackson School of Geosciences, University of Texas at Austin, J. J. Pickle Research Campus Building 196, 10100 Burnet Road (R2200), Austin, TX 78758, USA. (arbic@ig.utexas.edu)

D. R. MacAyeal, Department of Geophysical Sciences, University of Chicago, Chicago, IL 60637, USA.

G. A. Milne, Department of Earth Sciences, University of Ottawa, Ottawa, ON K1N 6N5, Canada.

J. X. Mitrovica, Department of Physics, University of Toronto, Toronto, ON M5S 1A7, Canada.